EXPERIMENTAL STUDY OF SMECTITE INTERACTION WITH METAL Fe AT LOW TEMPERATURE: 1. SMECTITE DESTABILIZATION

SÉBASTIEN LANTENOIS[1],*, BRUNO LANSON[2], FABRICE MULLER[1], ANDREAS BAUER[3], MICHEL JULLIEN[4] AND ALAIN PLANÇON[1]

[1] Institut des Sciences de la Terre d'Orléans (ISTO), CNRS − Université d'Orléans, 1A rue de la Férollerie, 45071 Orléans Cedex 2, France
[2] Environmental Geochemistry Group, LGIT, Maison des GéoSciences, Université J. Fourier − CNRS, BP 53, 38041 Grenoble Cedex 9, France
[3] Institut für Nukleare Entsorgung, Forschungzentrum Karlsruhe, PO Box 3640, 76021 Karlsruhe Germany
[4] Commissariat à l'Energie Atomique (CEA), Centre d'Etude de Cadarache DEN/DTN/SMTM/Laboratoire de Modélisation des Transferts dans l'Environnement, Bat 307, 13108 Saint Paul Lez Durance Cedex, France

Abstract—Interaction between metal Fe and a variety of natural and synthetic smectite samples with contrasting crystal chemistry was studied by scanning electron microscopy and X-ray diffraction from experiments conducted at 80ºC. These experiments demonstrate an important reactivity contrast as a function of smectite crystal chemistry. An XRD method involving the use of an internal standard allowed quantification of the relative proportion of smectite destabilized as a function of initial pH conditions as well as of smectite structural parameters. In mildly acidic to neutral pH conditions, a significant proportion of metal Fe is corroded to form magnetite without smectite destabilization. Under basic pH conditions, smectite and metal Fe are partly destabilized to form magnetite and newly-formed 1:1 phyllosilicate phases (odinite and crondstedtite). More specifically, systematic destabilization of both metal Fe and smectite is observed for dioctahedral smectites while trioctahedral smectites are essentially unaffected under similar experimental conditions. In addition, smectite reactivity is enhanced with increasing Fe^{3+} content and with the presence of Na^+ cations in smectite interlayers. A conceptual model for smectite destabilization is proposed. This model involves first the release of protons from smectite structure, $Me Fe^{3+}OH$ groups being deprotonated preferentially and metal Fe acting as proton acceptor. Corrosion of metal Fe results from its interaction with these protons. The Fe^{2+} cations resulting from this corrosion process sorb on the edges of smectite particles to induce the reduction of structural Fe^{3+} and migrate into smectite interlayers to compensate for the increased layer-charge deficit. Interlayer Fe^{2+} cations subsequently migrate to the octahedral sheet of smectite because of the extremely large layer-charge deficit. At low temperature, this migration is favored by the reaction time and by the absence of protons within the di-trigonal cavity. Smectite destabilization results from the inability of the tetrahedral sheets to accommodate the larger dimensions of the newly formed trioctahedral domains resulting from the migration of Fe^{2+} cations.

Key Words—Clay Barrier, Clay Stability, Engineered Barrier, Fe−clay Interactions, Fe Corrosion, Nuclear Waste Disposal, Smectite, X-ray Diffraction.

INTRODUCTION

In some of the 'multi-barrier' concepts envisaged for the storage of high- and intermediate-level and/or long-lived nuclear waste, metallic containers filled with vitrified nuclear waste are placed in a confinement barrier, which itself is surrounded by a geological barrier. The reactive components of the engineered and geological barriers are clays (mainly smectites) while metallic containers could be made up of Fe. To predict the long-term properties of these clay barriers, it is thus essential to study the interactions between clay minerals, and more especially smectite, and metal Fe as the corrosion of the metallic canister could in turn induce the destabilization of the clay minerals.

Studies of these Fe−clay interactions have indeed shown the partial but systematic destabilization of the initial clay material and the subsequent crystallization of reaction products (Habert, 2000; Perronnet, 2001, 2004; Kohler, 2001; Lantenois, 2003; Guillaume *et al.*, 2003). The nature of these reaction products depends on experimental conditions such as temperature and, to a minor extent, the nature of the initial clay material. When smectite is used, Fe-rich chlorite-like species are synthesized at high temperature (300ºC, Guillaume *et al.*, 2003) whereas Fe-rich serpentine-like species are obtained for temperatures more realistic in the context of nuclear waste disposal (80ºC, Habert, 2000; Perronnet, 2001, 2004; Lantenois, 2003). Newly formed 1:1 phyllosilicates with low Fe content were also identified by Kohler (2001) after reaction between Fe metal and kaolinite/smectite mixtures at 80ºC. As reaction pathways appear to vary significantly as a function of temperature (Guillaume *et al.*, 2003; Lantenois, 2003), it is especially important to work at temperatures similar to those expected during storage lifetimes, thus generally excluding medium-to-high temperature experiments

* E-mail address of corresponding author:
sebastien.lantenois@univ-orleans.fr

597

(>200°C). Other experimental conditions have been chosen to mimic those of the repository, and experiments were thus performed in an anoxic and reducing environment. The clay materials used for this study were essentially natural smectites which have swelling and self-healing abilities and cation retention properties suitable for engineered barriers. To promote the reactivity of clays so that significant reaction progress could be obtained on a laboratory-compatible timescale, the water/solid ratio was significantly increased.

A method has been developed to quantify the amount of smectite destabilized as a result of its interaction with metal Fe. The aim of the present study was to determine the role of the nature of clay minerals on the contrasting reactivity observed during their hydrothermal reaction with Fe metal by using a variety of starting materials. Specifically, the structural characteristics responsible for these differences were sought, together with the mechanism of clay destabilization. A companion paper will describe the crystal-chemistry of newly-formed phases.

MATERIALS AND METHODS

Materials

A variety of natural and synthetic smectite samples with contrasting crystal chemistry was used. These samples were selected to include both di- and tri-octahedral varieties, smectite with octahedral or tetrahedral substitutions, and to cover a wide range of chemical composition, focusing on the Fe content. The chemical compositions of selected samples are reported in Table 1. Untreated bulk samples were ground in an agate mortar to increase their reactivity, but samples were neither size-fractionated nor purified.

Synthetic clays were crystallized from gels under hydrothermal conditions. Gels were prepared following a method adapted from Hamilton and Henderson (1968) using tetraethyl orthosilicate (TEOS), $Mg(NO_3)_2.6H_2O$, $Al(NO_3)_3.9H_2O$, $Fe(NO_3)_3.9H_2O$, HNO_3, Na_2CO_3, NH_4OH and ethanol. All reagents had a 99% minimum grade. After dissolution of Al and Mg nitrates and of Na_2CO_3 in nitric acid, TEOS and ethanol were added. A precipitate was obtained by neutralizing the resulting solution at pH $\approx$ 6 with addition of NH_4OH. This precipitate was dried at 80°C for 24 h, ground in an agate mortar and heated to 400°C to remove nitrates and carbonates and to obtain a gel composed essentially of Al, Mg, Si and Na oxides. SapFe08 saponite was synthesized from such gels in a cold-sealed pressure vessel. Gel and deionized water were introduced in a 2:1 weight ratio in a silver tube which was itself placed in the vessel heated at 400°C for 1 month at an estimated pressure of 100 MPa (Suquet *et al.*, 1977). The SbS-1 beidellite was synthesized in an internally heated pressure vessel. 600 mg of gel were mixed to 1.3 g of a NaOH solution (0.2 N) in a gold tube. The tube was then sealed and heated to 350°C under 22 MPa for 10 days (Kloprogge *et al.*, 1999). After cooling of the vessels, the solid products were extracted from the

Table 1. Chemical composition of the initial smectite materials (structural formulae calculated per $O_{10}(OH)_2$) and relative proportion of smectite destabilized after reaction with metal Fe for 45 days.

Sample Nature[e]	Garfield[a] N	SWa-1[a] FS	Drayton[b] B	CP4[b] B	SbId[c] B	SbS-1[c,d] B	SWy-2[c] M	SAz-1[c] M	SapCa-2[c] S	SapFe08[c,d] S
Tetrahedral										
Si	3.51	3.70	3.69	3.60	3.71	3.66	3.95	4.00	3.58	3.62
Al	0.49	0.30	0.31	0.40	0.29	0.34	0.05	–	0.39	–
Fe^{3+}	–	–	–	–	–	–	–	–	0.03	0.38
charge	−0.49	−0.30	−0.31	−0.40	−0.29	−0.34	−0.05	–	−0.42	−0.38
Octahedral										
Al	0.11	0.55	1.11	1.70	1.80	2.00	1.56	1.37	–	–
Fe^{3+}	1.86	1.31	0.47	0.30	0.12	–	0.21	0.07	–	0.00
Mg	0.02	0.13	0.44	–	0.08	–	0.23	0.56	3.00	3.00
occupancy	1.99	1.99	2.02	2.00	2.00	2.00	2.00	2.00	3.00	3.00
charge	−0.05	−0.16	−0.38	0.00	−0.08	0.00	−0.23	−0.56	0.00	0.00
Interlayer										
Na	0.09	0.06	–	–	0.08	0.33	0.14	0.05	0.34	0.39
Ca	0.19	0.20	0.17	0.15	0.10	–	0.05	0.24	0.05	–
Mg	–	–	0.18	–	–	–	–	–	–	–
K	0.04	0.05	–	0.09	0.08	–	0.01	0.01	0.02	–
charge	0.51	0.51	0.70	0.39	0.36	0.33	0.25	0.54	0.46	0.39
Smectite destab. (wt.%)	95	90	70	40	60	0	50	20	0	0

[a] From Gates *et al.* (2002). Interlayer composition of raw materials was determined from electron microprobe analysis
[b] EDX analysis on a TEM, [c] electron microprobe analysis, [d] synthetic clays. [e] N, FS, B, M, S correspond to nontronite, ferruginous smectite, beidellite, montmorillonite and saponite, respectively

reaction tubes, dried at 80ºC overnight, and ground before structural and chemical characterization using X-ray diffraction (XRD) and energy dispersive X-ray fluorescence spectroscopy (EDS) on a transmission electron microscope (TEM).

To assess the role of the interlayer composition on the reaction rate better, K-, Na- and Ca-saturated specimens were prepared for samples SWy-2, Garfield and SAz-1. The cation-exchange procedure was performed at room temperature by immersing the ground clay sample in 1 M KCl, NaCl or CaCl$_2$ aqueous solutions. After 12 h of contact, the solid was extracted by centrifugation. The saturation procedure was repeated four times. The excess chloride was then removed by washing the sample five times with distilled water (K- and Ca-saturated samples). Na-saturated samples were washed once in ethanol and then dialyzed in deionized water for 1 week.

Experimental

For the Fe−clay interactions, 0.6 g of the clay powder were mixed with 0.6 g of metal Fe powder (10 μm maximum size, Merck® product for analysis) to maximize the contact surface between the Fe and clay particles. The large amount of metal Fe was also intended to promote reducing conditions during the experiments. 30 mL of water were added to this initial mixture. Deionized water (with a resistivity >18 MΩ cm^{-1}) was used to permit study of the final solution composition. Samples were prepared in an MBraun® glove box equipped with Cu catalysts to eliminate O$_2$, and an MBraun® O$_2$ control system. The partial pressure of O$_2$ was <1 ppm during sample preparation. Deionized water was degassed with Ar for 1 h prior to its introduction in the glove box and all products were allowed to stay in the glove box for 24 h to equilibrate with the glove box atmosphere. Starting products were then placed in 40 mL Nalgene® reactors. Because these reactors are oxygen porous, a 'double enclosure system' was used where the Nalgene® reactors were inserted into larger Teflon® reactors which contain metal Fe powder, FeSO$_4$ and water. Any oxygen entering the Teflon reactors was thus eliminated according to reactions 1 and 2 with ferrous and metal Fe, respectively (Aogaki, 1999).

$$2Fe^{2+} + 1/2O_2 + 3H_2O \rightarrow 4H^+ + 2FeOOH \qquad (1)$$
$$2Fe^o + 3/2O_2 + 3H_2O \rightarrow 2Fe(OH)_3 \qquad (2)$$
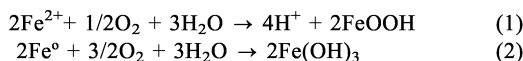
The two reactors were closed tightly within the glove box and subsequently heated at 80ºC for 45 days outside of the glove box. Additional experiments were also performed for 5, 15, 30, 60, 90 and 120 days on selected samples (Garfield, SbId, SWy-2 and SapCa-2). At the end of the reactions, the reactors were cooled to room temperature and opened in air, the solution pH being measured immediately. The solution was subsequently filtered (0.45 μm) and acidified for chemical analysis, whereas the solid fraction was dried at 80ºC overnight and ground.

Filtered solutions were analyzed for major and trace elements (Si, Al, Fe, Mg, Ti, Na, Ca and K) using an ICP-AES Jobin-Yvon ULTIMA spectrometer. Scanning electron microscopy (SEM) was performed using a JEOL 6400 microscope. Samples were covered with a Au film before observation to avoid charge build up. The TEM was performed using a JEOL 2000 FX microscope operated at 200 kV. Samples were prepared as a suspension in deionized water, a drop of this suspension being dried on copper grids covered with a carbon film.

Powder XRD patterns were recorded in transmission geometry using CoKα radiation (35 mA, 35 kV) to avoid Fe fluorescence. The use of an INEL CPS 120 curved, position-sensitive detector allowed simultaneous recording of the diffracted intensity over a 4−50º2θ range with a step size of 0.03º. The non-linearity of the detector was corrected (Roux and Wolfinger, 1996). A 0.5 mm diameter Lindemann glass tube was used to hold the sample powder.

Infrared (IR) spectra were recorded over the 650−4000 cm^{-1} range with a 2 cm^{-1} resolution using a Nicolet Magna-IR Fourier transform spectrometer equipped with a Globar SiC source and a DTGS detector. The spectrometer was purged with dry air prior to data collection to remove most of atmospheric H$_2$O. The sample was finely ground in an agate mortar, and 0.5 mg of the resulting powder were mixed to 150 mg of KBr previously dried at 120ºC for 24 h. The mixture was homogenized and pressed in an evacuable die to prepare a 12 mm diameter pellet. Decomposition of the IR spectra in the OH-bending region (700−900 cm^{-1}) was performed using the program Peak-Fit (v. 4.05).

The cation exchange capacity (CEC) was measured using the copper complex method (Gaboriau, 1991). 600 mg of sample were suspended for 12 h in 25 mL of a 0.02 N ethylene di-amine copper complex (Cu(EDA)$_2$Cl$_2$) solution. After centrifugation, the Cu concentration in solution was measured using a 905-GBC atomic absorption spectrophotometer from GBC Scientific Equipment.

Quantification of the relative proportion of smectite destabilized after reaction

To estimate reaction progress, the amount of residual smectite was quantified by XRD using the internal standard technique adapted for clays by Hillier (2000). As recommended by Hillier, each sample was mixed with 10% of a corundum internal standard (particle size <50 μm), dry ground in an agate mortar for 10 min and then introduced into the Lindeman glass tube. The use of a glass tube in transmission geometry allows optimization of the sample disorientation. Segregation due to particle size and/or particle density was minimized by careful grinding and mixing. Absorption corrections have not been considered because absorption, which is closely related to sample chemical composition, is similar before and after reaction.

The 001 reflection of smectite was not selected for quantification because its intensity depends strongly on smectite hydration state and thus on the chemical composition of smectite interlayers, which can be modified during the reaction. Instead, the amount of residual smectites was quantified by measuring the integrated intensity of the 02,11 peak (between 22.0 and 27.0°2θ CoKα Figure 1) before and after reaction, these intensities being normalized to the 012 reflection

of corundum (29.8°2θ CoKα; Figure 1). The background was assumed to be linear between 22.0 and 27.0°2θ and subtracted. If quartz impurities were present, the 100 reflection of quartz (~24.3°2θ CoKα) was fitted, and its integrated intensity subtracted from the total integrated intensity. To assess the validity of XRD results, the relative proportion of reacted smectite was also quantified from CEC measurements performed before and after reaction, the observed CEC decrease being directly
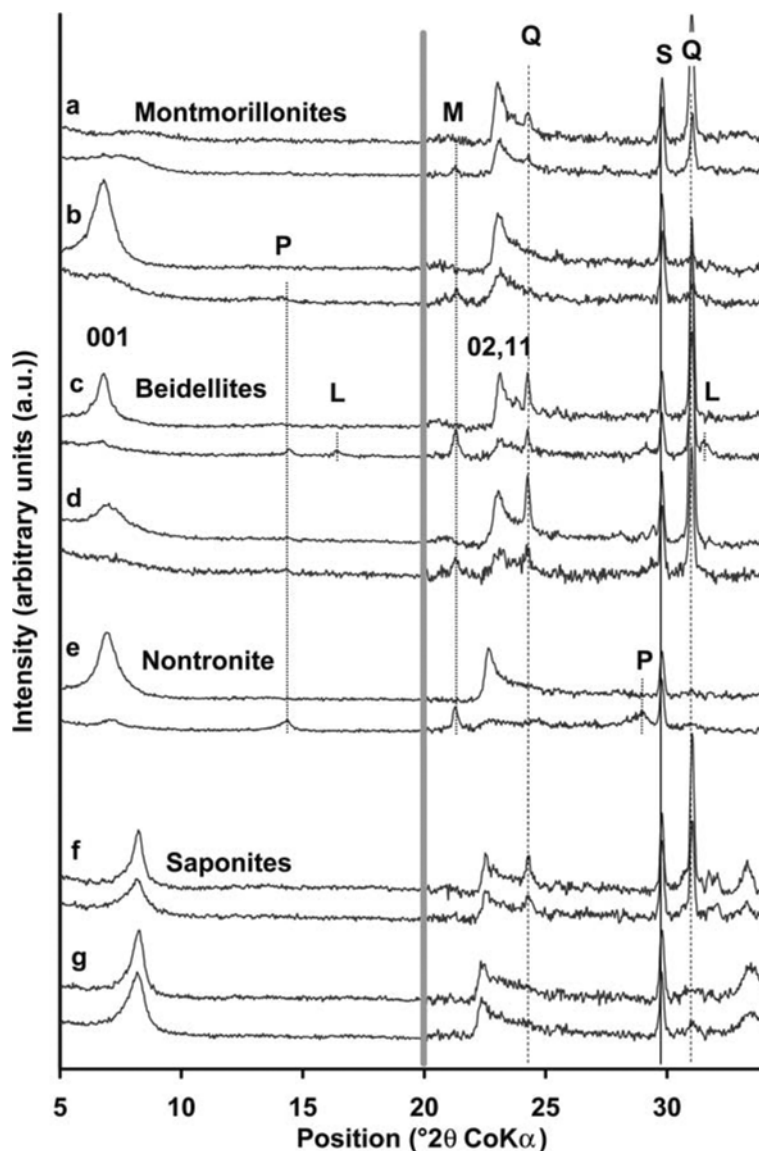
Figure 1. XRD patterns obtained on unreacted and reacted smectite samples (upper and lower patterns, respectively). Montmorillonite, beidellite, nontronite and saponite samples were reacted for 45 days with metal iron at 80°C (see text for details). (a) Sample SWy-2, (b) sample SAz-1, (c) sample SbId, (d) sample CP4, (e) sample Garfield, (f) sample SapCa-2, and (g) sample SapFe08. Scale factor (×3) over the 20−35°2θ CoKα range. Patterns were normalized by pairs to the integrated intensity of the corundum 012 reflection (solid line, S). The 001 reflection and the 02,11 reflection of the clay samples are labeled. Q indicates the presence of quartz impurities in some samples (dashed lines). Dotted lines indicate the reflections of newly-formed phases. These phases are labeled M, L and P for magnetite (Fe_3O_4), lepidocrocite (γ-FeOOH), and a newly-formed 1:1 phyllosilicate, respectively.

linked to the amount of destabilized smectite. This assumption was made possible by the non-swelling character of the reaction products (Lantenois, 2003).

The amount of residual smectite was also quantified using IR spectroscopy. Over the OH-bending frequency range, three bands at $912-920$ cm^{-1}, $874-886$ cm^{-1} and $840-850$ cm^{-1} correspond to the Al−Al−OH, Al−Fe−OH and Al−Mg−OH vibrations of smectites, respectively (Farmer, 1974; Goodman *et al.*, 1976; Russell and Fraser, 1994; Vantelon *et al.*, 2001). The position reported in the literature for the Fe−Fe−OH band scatters from $820-795$ cm^{-1} (Goodman *et al.*, 1976; Cuadros and Altaner, 1998) and overlaps with the Si−O vibrations of quartz at 780 and 800 cm^{-1} (Madejová and Komadel, 2001). To avoid using this problematic band, reaction progress was quantified using IR spectroscopy for Fe-poor smectites only. The quantification method itself requires subtracting a baseline which corresponds to Si−O vibrations in phyllosilicates (Figure 2a − Vantelon *et al.*, 2001). A cubic spline baseline, similar for all samples, was adjusted on both sides of the region of interest ($817-822$ cm^{-1} and $940-945$ cm^{-1}, respectively). The $822-945$ cm^{-1} range
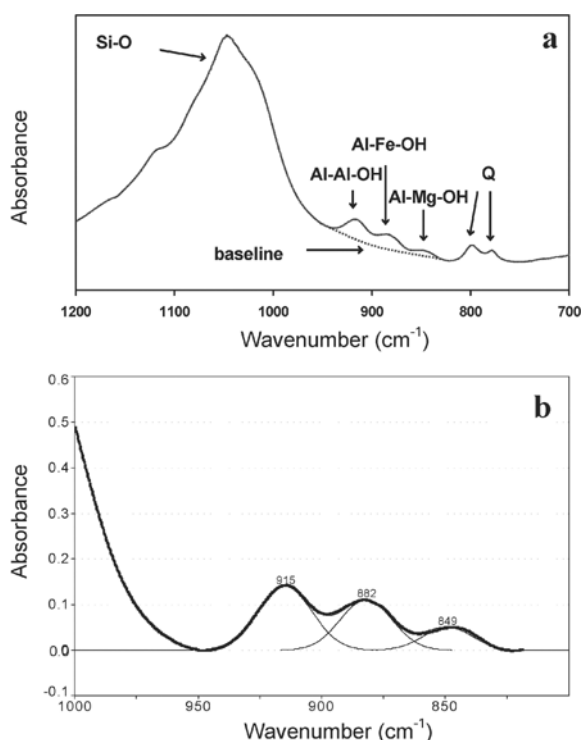

Figure 2. Method for quantifying the relative proportion of destabilized smectite using IR spectroscopy. (a) IR spectrum of sample SWy-2 (unreacted) before subtraction of the baseline. Si-O indicates the Si−O vibrations in phyllosilicates whereas Al−Al−OH, Al−Fe−OH and Al−Mg−OH refer to the OH-bending mode of the respective hydroxyl groups. Q denotes the two vibrations bands of quartz. (b) Decomposition assuming three Gaussian-shaped contributions of the OH-bending zone after baseline subtraction (sample SWy-2 unreacted).

of the baseline-corrected spectra was then fitted with three Gaussian-shaped curves (Figures 2b) corresponding to Al−Al−OH, Al−Fe−OH and Al−Mg−OH vibration modes. The relative proportion of unaltered smectite was estimated from the ratio between the total surface areas determined for these three contributions before and after reaction.

RESULTS

Qualitative evaluation of the reaction progress

Long-term experiments show that the reaction progress reaches a plateau after ~30 days (see below). Except when specifically notified, reactions described in the following section were thus performed for 45 days, without constraining the solution pH. The observed reaction depends on the nature of the initial smectite sample. In particular, di- and trioctahedral smectites exhibit contrasting reactivities and will be described separately.

Dioctahedral smectites. Although reaction progress varies considerably as a function of the initial smectite sample, a similar effect was observed for all dioctahedral smectites. After 45 days, solution pH was not significantly modified, whereas the chemical composition of the solutions was altered (Table 2). In particular, the concentration in solution of alkali and alkali-earth cations which were initially present in smectite interlayers (Na^+, Ca^{2+} and K^+) was significantly increased after reaction (Table 2) together with that of Si. For smectite samples reacted without metal Fe, Si was not detected in solution, and the concentration in solution of alkali and alkali-earth cations after reaction was lower than in similar experiments performed in the presence of metal Fe (Table 2). In all reacted samples, residual metal Fe was systematically present together with newly-formed phases (magnetite and 7 Å phyllosilicates; Figure 1a−e). However, Fe particles observed in all reacted samples appear corroded as compared to their initial state (Figure 3a,b). In addition, clay particles with a distinct morphology were observed in all reacted samples (Figure 3c). These particles probably correspond to the newly-formed phyllosilicate phase. Unreacted clay particles were also observed for both montmorillonite and beidellite samples (Figures 3d,e). Accordingly, residual smectite was identified for montmorillonite and beidellite samples from its 02,11 reflection at ~23°2θ CoKα (Figure 1a−d). The intensity of this characteristic reflection was much reduced after reaction for Garfield nontronite sample (Figure 1e), in agreement with the absence of unreacted clay particles in the reacted Garfield sample (Figure 3f).

Trioctahedral smectites. For saponite samples, solution pH and composition are not significantly modified after 45 days of Fe−clay interactions (Table 2). Accordingly,

Table 2. Chemical composition of the solution after reaction of smectite samples with metal Fe for 45 days.

	Si	Al	Fe	Mg	Na	Ca	K	Initial pH	Final pH
SapCa-2	0.0	0.0	0.0	0.0	10.0	4.0	0.0	9.5	10.0
SapCa-2 Ref	0.0	0.0	0.0	0.0	7.0	2.0	0.0	9.5	9.5
SWy-2	6.5	0.1	0.0	0.3	115	3.5	3.0	10.0	10.5
SWy-2 Ref	0.0	0.0	0.0	0.0	11.0	0.0	0.0	10.0	10.0
SbId	2.0	0.4	0.0	0.3	17.0	28.0	14.0	7.5	7.5
SbId Ref	0.0	0.0	0.0	0.0	1.0	2.0	1.0	7.5	7.5
Garfield	0.0	0.0	0.0	0.0	17.5	22.5	1.0	8.5	9.5
Garfield Ref	0.0	0.0	0.0	0.0	10.0	1.0	2.0	8.5	9.0

Concentrations are given in mg L^{-1}. Initial and final pH values were measured before and after reaction, respectively. Regular sample names correspond to the reaction of a given smectite sample with metal Fe for 45 days at 80°C. Ref samples correspond to the reaction of a given smectite sample for 45 days at 80°C without metal Fe.

XRD patterns recorded on both unreacted and reacted samples are alike (Figure 1f). In particular, the 02,11 peak (~23°2θ CoKα) is similar in both samples, and even the 001 reflection (~7°2θ CoKα) is practically unaffected. In addition, no extra reflection was visible after reaction. The SEM observations support this lack of reactivity as both Fe (not shown) and clay particles (Figure 3g,h) appear unaltered after 45 days.

Quantification of the extent of smectite destabilization

A quantitative estimate of the relative proportion of smectite destabilized after reaction was obtained from XRD results using the internal standard method (Hillier, 2000). Results of this quantification are presented in Table 1. The absolute precision on the relative proportion of smectite destabilized was estimated to be ±10%. This estimate corresponds to the standard deviation of 12 measurements obtained for 45 day experiments performed with sample SWy-2.

Using this quantitative XRD method it was possible to demonstrate the reactivity contrast as a function of the nature of initial smectite samples. For the different smectites presented in Figure 1, the relative proportion of destabilized smectite scatters from 0 to 95%. Trioctahedral smectites (SapCa-2 and SapFe08 samples) were essentially unaffected as a result of their interactions with Fe, while the dioctahedral smectites were systematically destabilized. Montmorillonite (20 and 50% of destabilized smectite for SAz-1 sample and SWy-2 samples, respectively) and beidellites (40, 60 and 70% of destabilized smectite for CP4, SbId and Drayton samples, respectively) were less destabilized than ferruginous smectites or nontronites (90 and 95% of destabilized smectite for SWa-1 and Garfield samples, respectively).

These quantification results were positively correlated to the estimates made using CEC measurements (Figure 4a). The precision of the CEC determination (±10%), which corresponds to the standard deviation of six measurements obtained for 45 day experiments performed with sample SWy-2, is similar to that of the XRD method. A good correlation was also obtained with the IR quantification results except for the Drayton sample (Figure 4b) which contains a significant proportion of ferric Fe (0.47 per $O_{10}(OH)_2$ − Table 1). Precision was estimated from the standard deviation of six measurements obtained for 45 day experiments performed with sample SWy-2. The IR measurements of reaction progress were found to be less precise (±15%) than those using XRD and CEC methods mostly as a result of the uncertainty on the baseline determination. In addition, note that IR results obtained on raw materials may be correlated with XRD data only in the absence of kaolinite which exhibits a band at 911 cm^{-1} which may interfere with the Al−Al−OH, Al−Fe−OH and Al−Mg−OH vibration modes.

For the three quantification methods, the possible influence of the newly-formed clay phases was neglected. This approximation was justified by the nature (crondstedtite, odinite) of the newly-formed phases (Lantenois, 2003). These 1:1 phyllosilicates were indeed non-swelling species thus exhibiting an extremely small CEC. As these phases contain a large amount of structural Fe, the 02,11 reflection of these Fe-rich 1:1 phyllosilicates was significantly shifted towards lower angles (at ~4.7 Å) as compared to the 02,11 reflection of initial smectite samples (at 4.45−4.56 Å for the whole compositional range). In addition, the intensity of the 02,11 peak of these Fe-rich 1:1 phyllosilicates was found to be extremely low, thus not significantly affecting the XRD measurements (Lantenois, 2003). The OH-bending bands observed for these Fe-rich 1:1 phyllosilicates were also shifted towards lower frequencies (750−800 cm^{-1}; Lantenois, 2003) as compared to initial Al-rich smectites (820−940 cm^{-1}).

Figure 3. (*facing page*) SEM images of unreacted and reacted samples. Metal Fe particles in unreacted and reacted SWy-2 sample are shown in (a) and (b), respectively. (c,d) Smectite particles in the reacted sample SWy-2. (e) Smectite particles in the initial sample SWy-2. (f) Smectite particles in the reacted Garfield sample. (g) Smectite particles in the initial sample SapCa-2. (h) Smectite particles in the reacted sample SapCa-2.
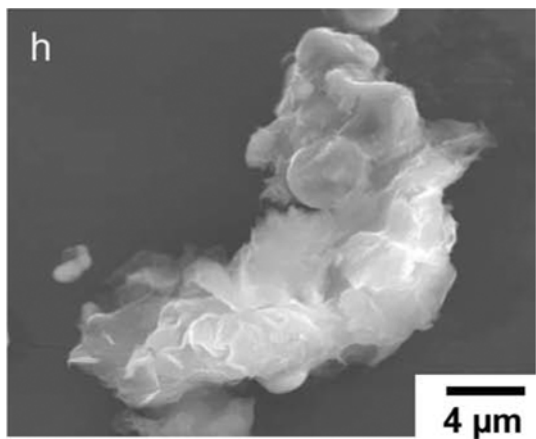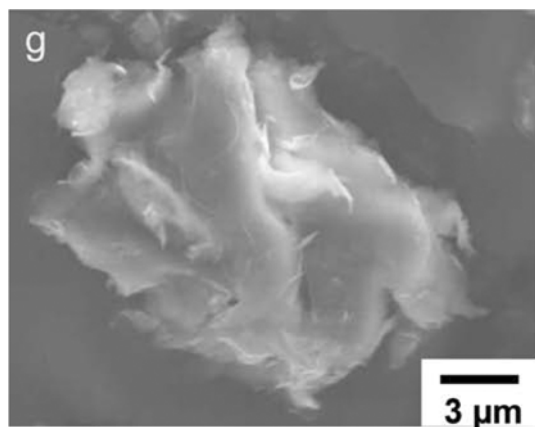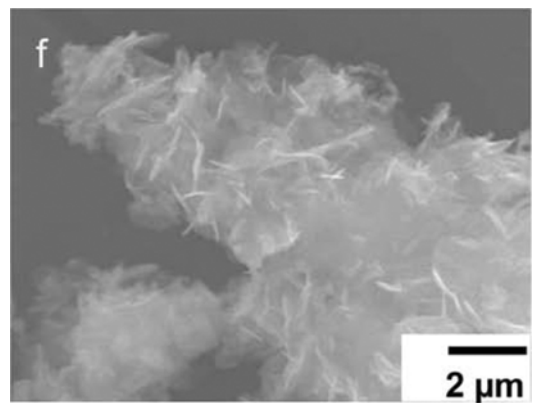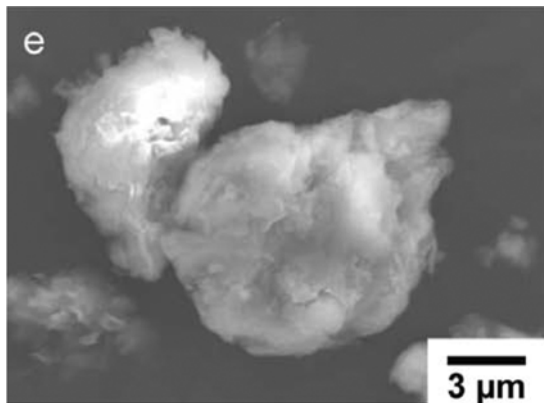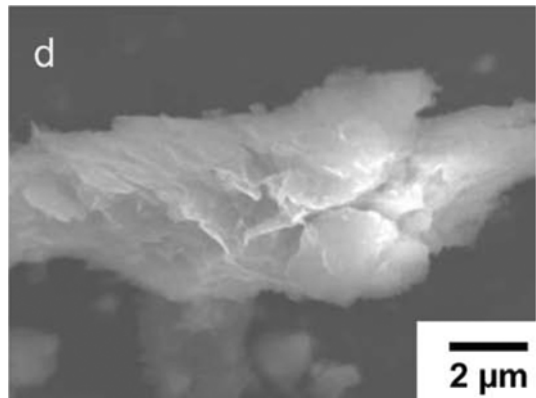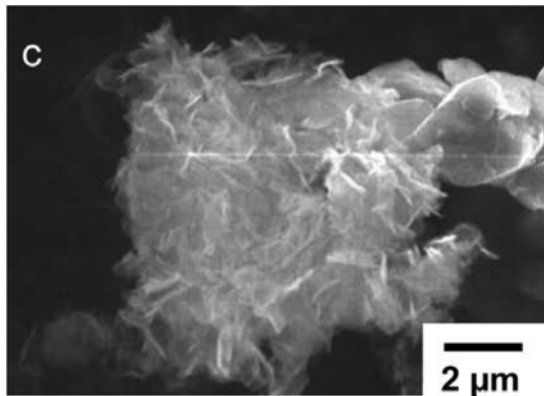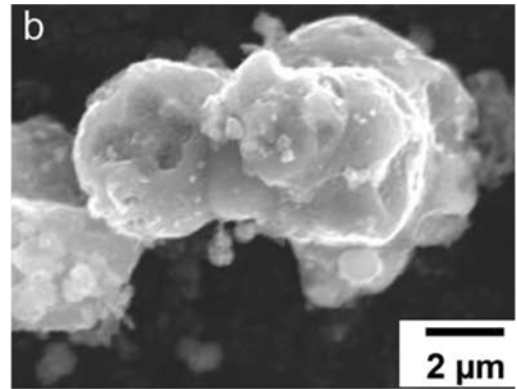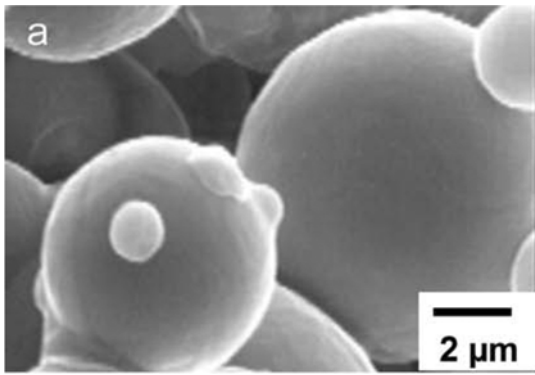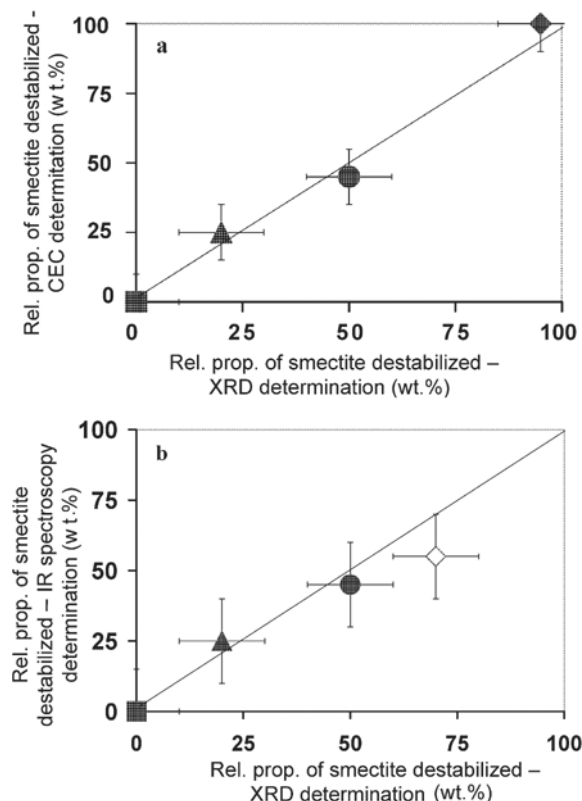
Figure 4. Relative proportion of destabilized smectite calculated by XRD and CEC methods (a) and by XRD and IR methods (b). Solid square: sample SapCa-2; solid triangle: sample SAz-1; solid circle: sample SWy-2; solid diamond: Garfield sample; open diamond: Drayton sample. The (1:1) line is shown as a solid line.

Kinetics of smectite destabilization

The XRD quantification of the relative proportion of smectite destabilized after reaction also allowed us to derive the kinetics of this destabilization reaction. For example, XRD patterns obtained for samples SbId reacted for 0, 5, 15, 30 and 45 days are presented in Figure 5. These experimental patterns are normalized to the 012 reflection of corundum so that the relative intensity of the 02,11 reflection can be compared for all samples. The relative proportion of smectite destabilized was estimated from the intensity decrease of this 02,11 peak as a function of reaction time (0−120 days). Results are plotted in Figure 6 for four samples (SbId, Garfield, SWy-2 and SapCa-2). As described qualitatively, no reaction was observed for sample SapCa-2. For dioctahedral smectites, the relative proportion of destabilized smectite increases with time to reach a steady-state plateau after 30−45 days. The amount of destabilized smectite obtained after 45 days can thus be considered as the final one for all smectites. As was observed qualitatively, the extent of smectite destabilization varies significantly as a function of the initial samples (50%, 60% and 95% of destabilized smectite for the SWy-2, SbId and Garfield samples, respectively).

DISCUSSION

Quantification by XRD of the relative proportion of destabilized smectite allows us to demonstrate that reaction progress depends heavily on the nature of the initial smectite sample, and that reaction kinetics cannot account for the reactivity contrast between different smectite samples. In the following discussion, the origin of these contrasting reactivities will be sought, and the influence of some structural characteristics of smectites
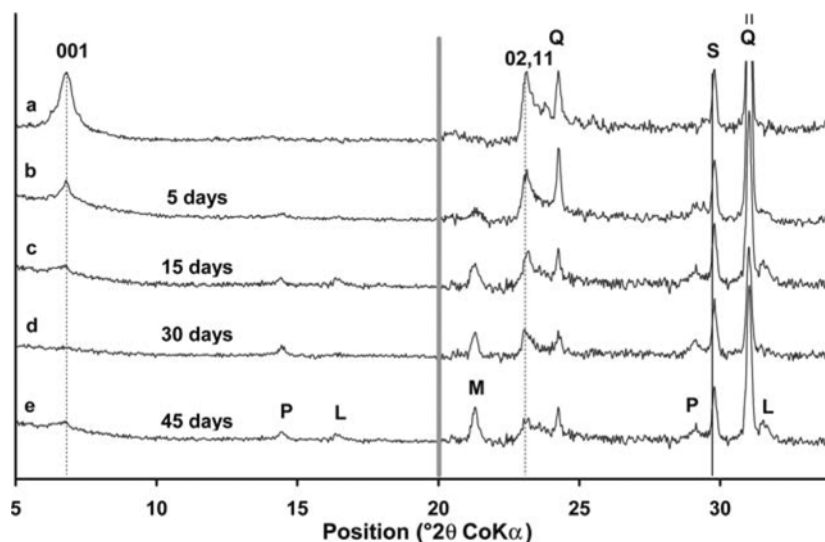

Figure 5. XRD patterns obtained for unreacted SbId sample (a) and for reacted SbId sample (b−e). (b, c, d, e) correspond to 5, 15, 30 and 45 day experiments, respectively. Scale factor (×3) over the 20−35°2θ CoKα range. Patterns were normalized as in Figure 1. Other labels and patterns as in Figure 1.
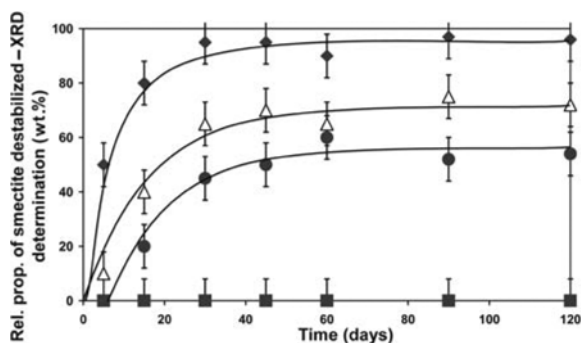
Figure 6. Evolution of the relative proportion of destabilized smectite as a function of reaction time. Symbols as in Figure 4. Open triangles: sample SbId.

will be discussed to hypothesize reaction mechanisms for the destabilization of smectite.

Influence of pH on smectite destabilization

The initial solution pH, which is obtained by equilibrating the different smectite samples in water, depends on the nature of the smectite, and varies from 7.5 to 10.5 (SbId-1 and SWy-2, respectively; Table 2). To assess the impact of this parameter on reaction progress, the relative proportion of destabilized smectite was determined as a function of the initial pH for sample SWy-2. The initial pH was adjusted by adding HCl or NaOH to the initial mixture. The relative proportion of destabilized smectite is reported in Table 3. When initial pH is basic (8−12 pH range), the nature of the reaction products and the reaction progress are independent of pH (Table 3). Conversely, the reaction is dramatically different when the initial pH is mildly acidic to neutral. In such a case, a large proportion of metal Fe is dissolved, whereas Fe oxides, identified as magnetite using XRD (data not shown), precipitate extensively. In addition, smectite appears unaffected (Table 3). A similar reaction, with the precipitation of magnetite and the stability of smectite, was observed for SapCa-2 and Garfield samples when initial pH was mildly acidic to neutral (Table 3).
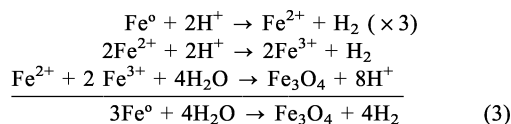
Under mildly acidic to neutral pH conditions such as those of the present study (pH = 6), smectite remains unaltered in the presence of metal Fe whatever its nature. However, smectite plays a catalytic role, because in the same experimental conditions (45 days, 80°C , initial

Table 3. Relative proportion of smectite destabilized (wt.%) as a function of the initial solution pH.

pH	SWy-2	SapCa-2	Garfield
6	0	0	0
8	50	–	95
10	50	0	–
12	50	–	–

Relative proportion of destabilized smectite is estimated using the XRD method.

pH = 6) metal Fe is not destabilized in the absence of smectite whereas in presence of smectite, metal Fe is oxidized, probably from its interaction with solution protons, to form magnetite according to the following reaction:

$$
\begin{array}{r}
Fe^o + 2H^+ \rightarrow Fe^{2+} + H_2 \ (\times 3) \\
2Fe^{2+} + 2H^+ \rightarrow 2Fe^{3+} + H_2 \\
\underline{Fe^{2+} + 2\ Fe^{3+} + 4H_2O \rightarrow Fe_3O_4 + 8H^+} \\
3Fe^o + 4H_2O \rightarrow Fe_3O_4 + 4H_2 \quad (3)
\end{array}
$$

In our experiments, the production of gaseous H_2 during the reaction was not observed as the Nalgene® reactors were H_2 porous.

Under more basic pH conditions (pH > 7 obtained from the addition of NaOH if necessary), the reaction is dramatically different as dioctahedral smectites are involved in the reaction. Dioctahedral smectites are then destabilized to form new clay phases according to the following reaction:

Metal Fe + smectite →
         1:1 Fe-rich phyllosilicate + Fe oxides   (4)

Under these basic pH conditions, destabilization of dioctahedral smectite is systematic but the amount of destabilized smectite varies significantly from one sample to the other probably as a function of the initial smectite crystal chemistry. Note that except for K-saturated smectites, the equilibration pH of smectite with water is basic. The pH is essentially unaffected by Fe−clay interactions.

Influence of smectite crystal chemistry on smectite destabilization

Influence of the di- or trioctahedral character. Although initial pH values are alike, and basic, for both di- and trioctahedral smectites, the reactivity of trioctahedral smectites is strikingly different from that of dioctahedral ones. Dioctahedral smectites are indeed systematically destabilized as the result of their interaction with metal Fe whereas trioctahedral smectites remain unaffected under similar experimental conditions (Figures 1, 6). This lack of reactivity is independent of the Fe content of trioctahedral smectites and of the nature of the interlayer cation.

Influence of structural Fe^{3+}. As can be seen in Figure 6 and in Table 1, nontronite and ferruginous smectites are thoroughly destabilized as the result of their interaction with metal Fe. In both cases, Fe^{3+} is the predominant cation in the octahedral sheet of these 2:1 expandable phyllosilicates which exhibit mostly tetrahedral substitutions (Table 1). By contrast, the extent of the destabilization is much reduced for smectites that are not Fe-rich, whatever the origin of the layer-charge deficit. However, this decrease in reactivity is less important for beidellites (tetrahedral layer charge) than for montmorillonites (octahedral layer charge) for a
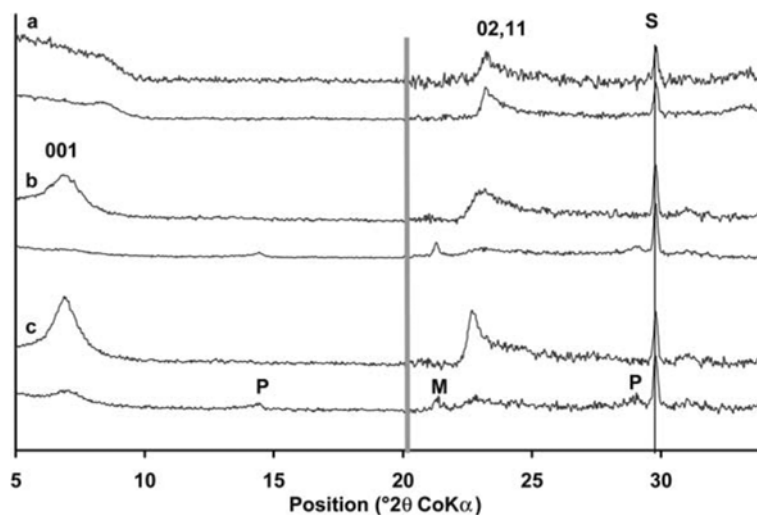
Figure 7. XRD patterns obtained on unreacted and reacted beidellite samples (upper and lower patterns, respectively). Patterns are ranked as a function of their structural Fe^{3+} content (Table 1). Samples were reacted for 45 days with metal Fe at 80ºC without controlling the initial pH. (a) Sample SbS-1, (b) Drayton sample, and (c) sample SWa-1. Scale factor ($\times 3$) over the $20-35º2\theta$ CoKα range. Patterns were normalized as in Figure 1. Other labels and patterns as in Figure 1.

given Fe^{3+} content. To illustrate further the influence of the amount of structural Fe on smectite destabilization, the XRD patterns of reacted and unreacted samples are compared in Figures 1 and 7 for dioctahedral smectites with predominant tetrahedral charges (beidellites). Their octahedral Fe^{3+} content ranges from 0.0 to 1.9 per $O_{10}(OH)_2$. The relative proportions of destabilized smectites are reported as a function of the Fe^{3+} content in Figure 8. No reaction is observed when no structural Fe^{3+} is present in dioctahedral smectites, and smectite is not destabilized (Figures 7a, 8). The presence of structural Fe^{3+} is thus an essential condition for the destabilization of dioctahedral smectites when in contact with metal Fe. The minimum amount of structural Fe^{3+} necessary to induce this destabilization is extremely small, as 60% of samples SbId are destabilized after 45 days of reaction with metal Fe, in spite of its limited

Fe^{3+} content (0.1 atom per $O_{10}(OH)_2$). In addition to this essential triggering role, the reactivity of dioctahedral smectite is clearly enhanced by an increased content of octahedral Fe^{3+} (Figure 8). However, this parameter is not the only structural parameter influencing smectite reactivity as, for example, the relative proportion of destabilized smectite is much greater for sample SbId than for sample CP4, in spite of the larger Fe^{3+} content in the latter sample (Figures 1c,d, 8, Table 1).

Influence of the interlayer cation composition. The cation composition of smectite interlayers appears as an additional parameter influencing the reactivity of dioctahedral smectites. All samples used in the experiments reported to this point were unprocessed, and Ca^{2+} was usually predominant in their interlayer spaces (Table 1). However, K^+ was also present in CP4 and SbId, whereas Na^+ was present in several samples (SbId, SWy-2, SAz-1), and Mg^{2+} in the Drayton sample. To assess the influence of the interlayer cation composition on smectite reactivity, three smectite samples (SWy-2, SAz-1 and Garfield) were reacted with metal Fe following their saturation with Na^+, Ca^{2+} and K^+. The XRD patterns of reacted SWy-2 samples are presented in Figure 9, whereas the relative proportions of smectite destabilized after 45 days of reaction with metal Fe are reported in Table 4. If Ca-saturated smectites are used as a reference, smectite destabilization is enhanced for Na-saturated smectites whereas it is decreased for K-saturated samples.

The reactivity contrast observed as a function of the interlayer cation composition is probably related to the hydration of smectite which varies as a function of the interlayer cation (Norrish, 1954; Pons *et al.*, 1981). The d_{001} basal spacing of K^+-saturated smectites varies from 12.5 to 15.5 Å in aqueous solution (Mamy, 1968; Besson
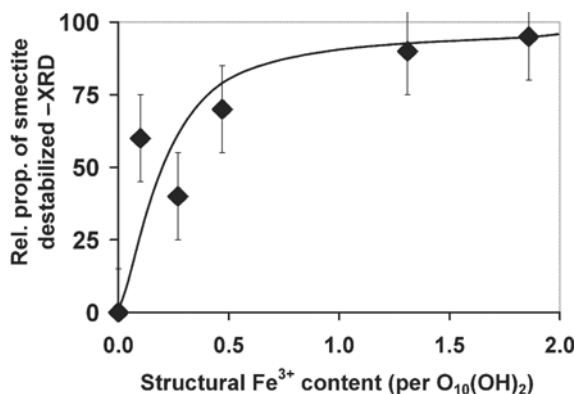

Figure 8. Relative proportion of destabilized smectite after reaction with metal Fe as a function of their content of structural Fe^{3+} (Table 1). The relative proportions of destabilized smectite were estimated using XRD in 45 day experiments.
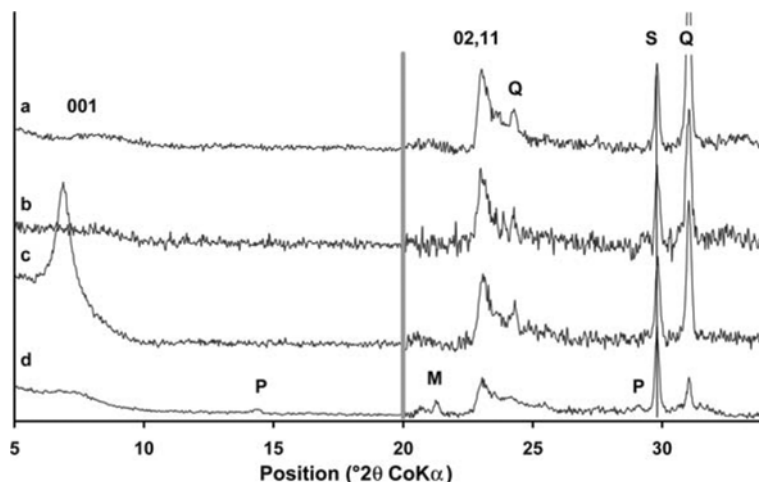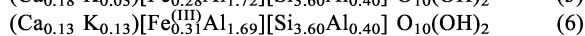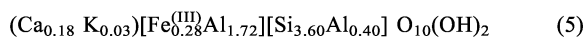
Figure 9. XRD patterns recorded on sample SWy-2 reacted with metal Fe after K, Ca and Na saturation (b, c and d, respectively). Unreacted Na-saturated sample corresponds to the raw SWy-2 sample (a). Scale factor ($\times 3$) over the $20-35°2\theta$ CoKα range. Patterns were normalized as in Figure 1. Other labels and patterns as in Figure 1.

and Tchoubar, 1980), whereas that of Ca^{2+}-saturated smectites varies from 18.6 to 19.2 Å (Suquet, 1978). The d_{001} basal spacing of Na^+-saturated smectites is not limited (osmotic swelling; Suquet et al., 1981). No significant collapse of smectite interlayers is expected as the ionic strength of the solutions, and more specifically the concentration of alkali and alkali-earth cations, remains small after reaction (Table 2). The enhanced reactivity observed for the most hydrated samples ($Na^+ > Ca^{2+} > K^+$) indicates that the ability of solution cations to access smectite interlayers is a key parameter to smectite destabilization.

Accordingly, the interlayer cation composition of samples CP4 and SbId is probably responsible for their contrasting reactivity which does not seem to be consistent with their respective Fe^{3+} contents (Figure 8, Table 1). Specifically, the presence of Na^+ in the interlayers of sample SbId probably enhances its reactivity as compared to sample CP4 in spite of the higher Fe content in the latter sample. The influence of the cation interlayer composition may also account for the different reactivity exhibited by populations of particles observed in sample CP4. Using TEM-EDX, two populations of particles were indeed differentiated from their morphology, as 'rolled' and 'flat' particles

and were identified in this sample (Figure 10). The chemical analysis of these two types of particles revealed that although the composition of the 2:1 layers was identical in both cases, the two populations differed by their interlayer cation composition as the following structural formulae were derived for 'rolled' and 'flat' particles, respectively (average values from twelve analyses):

$$(Ca_{0.18} K_{0.03})[Fe_{0.28}^{(III)}Al_{1.72}][Si_{3.60}Al_{0.40}] O_{10}(OH)_2 \quad (5)$$
$$(Ca_{0.13} K_{0.13})[Fe_{0.31}^{(III)}Al_{1.69}][Si_{3.60}Al_{0.40}] O_{10}(OH)_2 \quad (6)$$

After reaction with metal Fe, no remnant 'rolled' particles were observed and only 'flat' particles persisted. This is probably due to the increased proportion of K^+ in the interlayer of the latter particles which reduces their reactivity. Note that because long-term experiments were not performed on homoionic samples, it is not clear if the relative proportion of smectite

Table 4. Relative proportion of smectite destabilized (wt.%) as a function of the cation interlayer composition.

	SAz-1	SWy-2	Garfield
K	–	0	50
Ca	20*	20	95*
Na	40	50*	–

Relative proportion of destabilized smectite is estimated using the XRD method. * indicates raw samples, with the corresponding predominant interlayer cation.
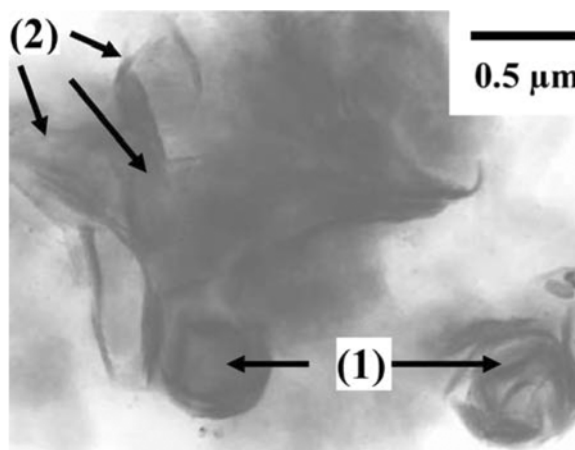

Figure 10. Transmission electron micrograph of smectite particles from sample CP4. 'Rolled' and 'flat' particles are labeled 1 and 2, respectively.

ultimately destabilized varies from one cation to the other, or if the nature of the interlayer cation essentially influences the destabilization rate.

Towards a possible model for smectite destabilization

Experimental constraints. From the above observations, several structural features appear essential to the destabilization of smectite when in contact with metal Fe. First, the smectite should be dioctahedral and should contain octahedral Fe^{3+}. In addition, the accessibility of its interlayer space is a key parameter for the apparent reactivity of the dioctahedral smectite. Finally, when comparing experiments run at different pH values, structural protons of the smectite are probably involved in the oxidation of metal Fe under neutral-to-alkaline conditions. In mildly acidic to neutral conditions, solution protons are abundant enough so that smectite is used essentially as a catalyst but is not directly involved in the corrosion of Fe following reaction 3. Under high pH conditions, protons are essentially present as OH groups in smectite, as both smectite interlayer and edge sites are essentially deprotonated under such pH conditions.

Deprotonation of these hydroxyl groups may occur under a variety of physico-chemical conditions for dioctahedral smectites (Russell, 1979; Jaynes and Bigham, 1987; Heller-Kallai and Rozenson, 1981; Heller-Kallai, 2001; Figure 11a). In particular, the presence of inorganic proton acceptors, usually alkali halides or alkali hydroxides, has been reported to induce such a deprotonation reaction (Heller-Kallai, 1975a, 1975b, 2001; Russell, 1979; Heller-Kallai and Rozenson, 1981; Heller-Kallai and Mosser, 1995). In our case, metal Fe is probably the proton acceptor triggering smectite deprotonation. Metal Fe is oxidized in turn as the result of its interaction with protons (Figure 11b) according to reaction 3. The high affinity of metal Fe for smectite and their resulting interactions have, for example, been recognized as causing the oxidation of steel pipes when using clay-containing drilling fluids (Tomoe *et al.*, 1999; Cosultchi *et al.*, 2003). According to this model, both the oxidation of metal Fe and the deprotonation of smectite are strongly favored by the accessibility of metal Fe to smectite interlayers. In this respect, the osmotic swelling commonly observed for Na-saturated smectites significantly enhances the accessibility of metal Fe particles to smectite interlayers, thus favoring the deprotonation reaction. In turn, deprotonation increases considerably the layer charge deficit in the smectite octahedral sheet and thus enhances their reactivity.

Deprotonation thus appears as the driving force for the oxidation of metal ions, and for the initiation of smectite destabilization. Accordingly, the presence of Fe^{3+} in the octahedral sheet of smectite appears as an essential parameter for these two reactions as $Me\mathrm{Fe}^{3+}$OH groups are known to deprotonate preferentially in dioctahedral smectites (Heller-Kallai, 1975a, 2001;
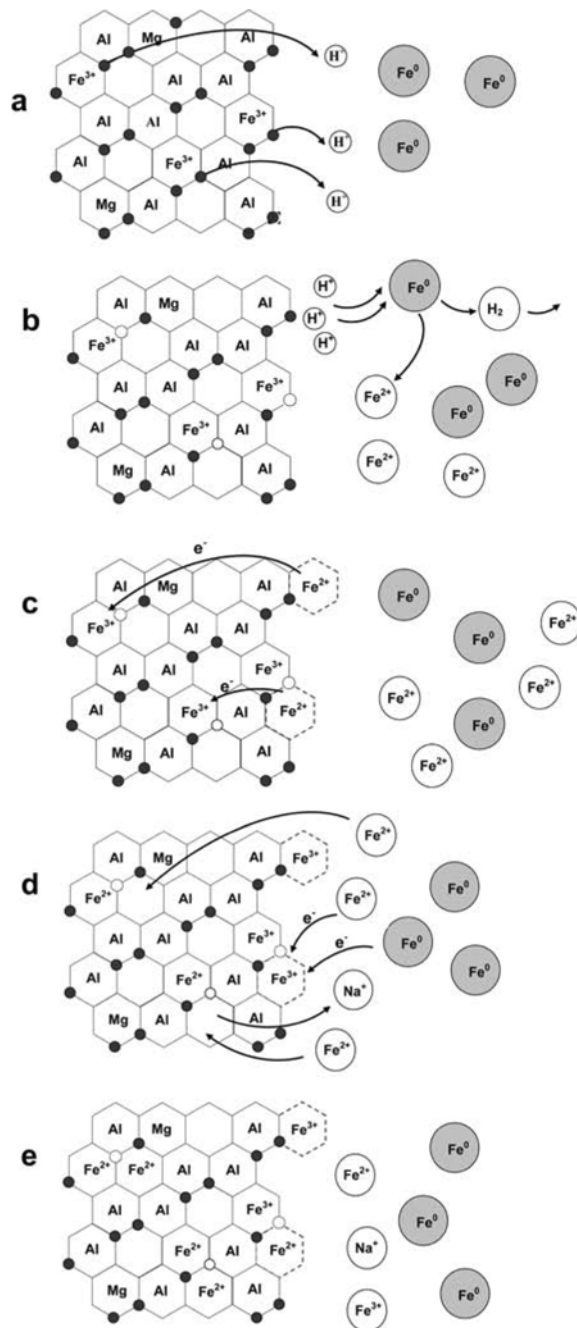

Figure 11. Conceptual model leading to the destabilization of dioctahedral smectites as a result of their interaction with metal Fe. (a) Deprotonation of $Me\mathrm{Fe}^{3+}$OH groups. (b) Oxidation of metal Fe as a result of its interaction with released protons. (c) Sorption of Fe^{2+} cations on the edges of smectite particles and reduction of structural Fe^{3+} cations. (d) Migration of solution Fe^{2+} cations in smectite interlayers to compensate for the layer charge deficit. Part of this migration results from an Fe^{2+}-for-Na^+ exchange. With time, interlayer Fe^{2+} cations migrate to the di-trigonal cavity and further to the octahedral sheet to compensate locally for the charge deficit. (e) Coexistence of di- and trioctahedral domains in the octahedral sheet of smectite leads to its destabilization.

Russell, 1979; Jaynes and Bigham, 1987). It is not clear, however, if deprotonation of Fe^{3+}-free dioctahedral smectites is not occurring, or is extremely limited, or if deprotonation is not the limiting step for the destabilization of Fe^{3+}-free dioctahedral smectites. Although Heller-Kallai (1975a) showed that deprotonation occurs even in Fe^{3+}-free dioctahedral smectite, we have not observed Fe corrosion resulting from this process in the experiments with sample SbS-1.

Destabilization of smectite. Following its initial deprotonation, destabilization of smectite is probably favored by the presence of Fe^{2+} in solution as a result of the oxidation of metal Fe. Specifically, the high affinity of Fe^{2+} for smectite edge surface sites (Tournassat *et al.*, 2005, Figure 11c) is probably a key factor for the subsequent destabilization of smectite. Following their sorption on these edge sites, Fe^{2+} cations are readily oxidized as shown by Tournassat *et al.* (2005), the electron acceptors being octahedral Fe^{3+} from smectite structure (Figure 11c). Note that following their oxidation, sorbed Fe cations may also accept electrons either from solution Fe^{2+} cations or from Fe metal to restore their 2+ valency (Figure 11d). As a result of both its initial deprotonation and of the subsequent reduction of its structural Fe^{3+}, the charge deficit in the octahedral sheet of smectite is dramatically increased and Fe^{2+} cations probably migrate in its interlayers to compensate for the increased layer charge (Figure 11d). The increased concentration of Fe^{2+} in solution resulting from the oxidation of the metal Fe also favors an Fe^{2+}-for-Na^+ cation exchange. Such Fe^{2+}-for-Na^+ cation exchange has been shown to occur in reducing environments (Kamei *et al.*, 1999).

The effective ionic radius of Fe^{2+} cations (0.78 Å — Shannon, 1976) is smaller than the maximum size allowing migration of the cations into the silicate layer approximated by Heller-Kallai (2001) at 0.85 Å. It is thus likely that interlayer Fe^{2+} cations actually migrate either into the di-trigonal cavities of smectite tetrahedral sheets or into the smectite octahedral sheets (Figure 11e). This migration is similar to that of Li^+ cations (0.76 Å — Shannon, 1976) involved in the Hofmann-Klemen test (Hofmann and Klemen, 1950; Greene-Kelly, 1955). The migration of Li^+ from the interlayer to the di-trigonal cavity and further to the octahedral sheet of montmorillonites has been extensively documented (Hofmann and Klemen, 1950; Greene-Kelly, 1955; Glaeser and Fripiat, 1976; Madejová *et al.*, 1996, 2000a, 2000b, among others). Heating to 300°C for 24 h represents the optimum experimental conditions for this migration. Migration of other divalent cations with an effective ionic radius similar to that of Li^+ cations has also been described. For example, Cu^{2+}, Ni^{2+} and Zn^{2+} cations (0.73, 0.69 and 0.74 Å, respectively) migrate from montmorillonite interlayers to the di-trigonal cavity between 100 and

300°C (Heller-Kallai and Mosser, 1995; Mosser *et al.*, 1997; Madejová *et al.*, 1999; Palkova *et al.*, 2003) and to the octahedral sheet at higher temperature (Brindley and Ertem, 1971; McBride and Mortland, 1974; Heller-Kallai and Mosser, 1995; Emmerich *et al.*, 1999). These conditions are much more energetically favorable than those involved in our experiments. However, partial migration of Li at least to the di-trigonal cavity has been reported for Li-saturated montmorillonite heated to 105°C for 24 h (Madejová *et al.*, 1996).

In our experiments, three factors compensate for the low thermal energy available. The first is the extremely strong layer-charge deficit which, according to the structural model proposed for smectite destabilization occurring in our experiments, arises both from the deprotonation of hydroxyl groups and from the reduction of structural Fe^{3+}. Note that the need for an octahedral layer-charge deficit is the fundamental basis for the migration of Li^+ cations involved in the Hofmann-Klemen test (Hofmann and Klemen, 1950). Furthermore, the positive influence of an increased layer charge deficit on the migration of divalent cations has been reported by Heller-Kallai and Mosser (1995). These authors observed an increased amount of Cu in samples that were deprotonated first. As described by Heller-Kallai and Mosser (1995), the positive effect of the initial deprotonation is not restricted to the increased layer-charge deficit and the second factor favoring the migration of Fe^{2+} cations is the absence of protons inside the di-trigonal cavity. As a consequence, there is no electrostatic repulsion to the migration of Fe^{2+} cations into the octahedral sheet. The reaction time represents the third factor compensating for the low thermal energy in our experiments. Our experiments lasted for 45 days whereas the common duration of experiments leading to the formation of reduced-charge smectites is 24 h. Initial migration of Fe^{2+} cations to the di-trigonal cavity is probably favored by an increased undersaturation of the oxygen atoms present at the surface of the 2:1 layers, *i.e.* by the existence of layer-charge deficit in smectite tetrahedral sheets. Such a location of the layer-charge deficit indeed favors the initial partial dehydration of interlayer Fe^{2+} cations, allowing for the formation of an inner-sphere complex necessary for their migration, and thus accounts for the increased reactivity of beidellite samples as compared to montmorillonite ones for a given Fe content (see samples SAz-1 and SbId — Table 1). The formation of such inner-sphere complexes has been widely documented in hydrated beidellites for monovalent interlayer cations, both from XRD (Ben Brahim *et al.*, 1983a, 1983b, 1984), and IR (Pelletier *et al.*, 2003) studies, and from Monte-Carlo modeling (Chang *et al.*, 1995; Skipper *et al.*, 1995).

In our experiments, migration of Fe^{2+} cations in the octahedral sheet of smectite does not induce a collapse of smectite interlayers as these new octahedral Fe^{2+} ions essentially compensate for the layer-charge deficit

resulting from the deprotonation of hydroxyl groups and from the reduction of structural Fe^{3+}, but not for the initial charge deficit of the 2:1 layers. The presence of hydrated interlayer cations, part of which are Fe^{2+}, still compensates for this initial charge deficit, and keeps the smectite interlayers expanded. The migration of Fe^{2+} cations in the octahedral sheet of smectite is rather thought to be responsible for the destabilization of smectites induced by their interaction with metal Fe. Destabilization is indeed thought to result from the presence of trioctahedral domains in the octahedral sheet of reacted smectite (Figure 11e). The coexistence of both dioctahedral and trioctahedral domains is widely reported in natural 1:1 phyllosilicates but is limited in 2:1 phyllosilicates (Bailey, 1980). The existence of 2:1 phyllosilicates with a mixed di- and trioctahedral occupancy is essentially limited to mica species exhibiting a tetrahedral charge (muscovite–zinnwaldite or muscovite–phlogopite series − Monier and Robert, 1986). In such species, the increased dimensions of the octahedral sheet in the *ab* plane are accommodated by the reduction of the tetrahedral tilt angle. In smectites, and more especially in montmorillonites, the amount of tetrahedral substitutions is limited and the initial tetrahedral tilt angle is thus minimal. As a consequence, such 2:1 phyllosilicates are unable to accommodate the presence of trioctahedral domains containing large cations and are thus destabilized by the migration of Fe^{2+} cations into their octahedral sheet.

According to the conceptual model hypothesized for smectite destabilization, the lack of reactivity of trioctahedral smectites results from three main factors. The first two are related to the absence of Fe^{3+} cations in the octahedral sheet of these smectite samples. The first effect of this absence is to make deprotonation of hydroxyl groups more difficult as, in dioctahedral smectites, MeFe^{3+}OH groups are known to deprotonate preferentially (Heller-Kallai, 1975a, 2001; Russell, 1979; Jaynes and Bigham, 1987). The second effect is the absence of cations that may be reduced in the octahedral sheet of trioctahedral smectites. The combination of these two effects prevents the building of a strong layer-charge deficit in the octahedral sheet of trioctahedral smectites. The third factor leading to the lack of reactivity of trioctahedral smectite is that it is obviously impossible for cations to migrate into this octahedral sheet which is fully occupied.

Influence of structural Fe on smectite destabilization. In the above conceptual model for smectite destabilization, the effect of an increased proportion of structural Fe on smectite destabilization is dual. The first effect arises from the increased proportion of MeFe^{3+}OH groups that will readily deprotonate when in contact with metal Fe. The larger number of deprotonated hydroxyl groups requires, in turn, the presence of a larger number of Fe^{2+} cations in smectite interlayers to balance the charge. The

second effect is directly related to the increased proportion of structural Fe^{3+} in the smectite octahedral sheet. This allows for a larger proportion of smectite octahedral sheets to present dramatic charge deficit leading to the migration of interlayer Fe^{2+} in the 2:1 layer, thus destabilizing it. On the other hand, the presence of Fe^{3+} in the smectite tetrahedral sheet does not enhance smectite reactivity as these cations cannot be reduced because of steric constraints arising from their tetrahedral environment.

CONCLUSIONS

The present study aimed to assess the stability of smectites which represent the reactive components of the engineered and geological barriers, when in contact with metal Fe at realistic temperatures in the context of nuclear waste disposal (80ºC). Dioctahedral smectites are thoroughly destabilized under such conditions, leading to the precipitation of magnetite and of 1:1 Fe-rich phyllosilicates (odinite, crondstedtite: Lantenois, 2003). Smectite destabilization is systematic for neutral-to-basic pH conditions (pH > 7), whereas in mildly acidic to neutral pH conditions, a significant proportion of metal Fe is corroded to form magnetite without smectite destabilization.

An XRD method was developed to quantify the extent of smectite destabilization. This method was validated against CEC measurements and IR spectroscopy results. In addition, structural and crystal-chemical factors favoring smectite destabilization were determined. These parameters include the amount of structural Fe, the presence of tetrahedral substitutions, and the nature of interlayer cations, and a conceptual model was hypothesized to account for smectite destabilization. According to this model, the formation of trioctahedral clusters resulting from the migration of Fe^{2+} cations into the octahedral sheet of the 2:1 layer is responsible for smectite destabilization as tetrahedral sheets are unable to accommodate the larger dimensions of these domains.

In agreement with experimental results, the dioctahedral character of the initial smectite is an essential condition for its destabilization in the proposed model. As a result, the non-reactivity of trioctahedral smectites appears to be an important point in the concept of engineered barriers for nuclear waste disposal, although natural deposits of trioctahedral smectite are uncommon.

present manuscript was improved by the constructive reviews of Lisa Heller-Kallaï, Will Gates and Associate Editor Peter Komadel.

REFERENCES

Aogaki, R. (1999) Non-equilibrium fluctuations in the corrosion. Pp. 217–305 in: *Modern Aspects of Electrochemistry* (R.E White, B.E. Conway and J.O'M. Bockris, editors). Kluwer, New York.

Bailey, S.W. (1980) Structures of layer silicates. Pp. 1–123 in: *Crystal Structures of Clay Minerals and their X-ray Identification* (G.W. Brindley and G. Brown, editors). Monograph **5**, Mineralogical Society, London.

Ben Brahim, J., Armagan, G., Besson, G. and Tchoubar, C. (1983a) X-ray diffraction studies on the arrangement of water molecules in a smectite. I. Homogeneous two-water-layer Na-beidellite. *Journal of Applied Crystallography*, **16**, 264–269.

Ben Brahim, J., Besson, G. and Tchoubar, C. (1983b) Layer succession and water molecules arrangement in a homogeneous two-water layer Na-smectite. Pp. 65–75 in: *Proceedings of the 5th Meeting of the European Clay Groups*, Prague.

Ben Brahim, J., Besson, G. and Tchoubar, C. (1984) Etude des profils des bandes de diffraction X d'une beidellite-Na hydratée à deux couches d'eau. Détermination du mode d'empilement des feuillets et des sites occupés par l'eau. *Journal of Applied Crystallography*, **17**, 179–188.

Besson, G. and Tchoubar, C. (1980) Exemple d'ordre-désordre par rotation des feuillets dans la montmorillonite potassique. *Bulletin de Minéralogie*, **103**, 429–433.

Brindley, G.W. and Ertem, G. (1971) Preparation and solvation properties of some variable charge montmorillonites. *Clays and Clay Minerals*, **19**, 399–404.

Chang, F.R.C., Skipper, N.T. and Sposito, G. (1995) Computer simulation of interlayer molecular structure in sodium montmorillonite hydrates. *Langmuir*, **11**, 2734–2741.

Cosultchi, A., Rossbach, P. and Hernandez-Calderon, I. (2003) XPS analysis of petroleum well tubing adherence. *Surface and Interface Analysis*, **35**, 239–245.

Cuadros, J. and Altaner, S.P. (1998) Compositional and structural features of the octahedral sheet in mixed-layer illite/smectite from bentonites. *European Journal of Mineralogy*, **10**, 111–124.

Emmerich, K., Madsen, F.T. and Kahr, G. (1999) Dehydroxylation behavior of heat-treated and steam-treated homoionic *cis*-vacant montmorillonites. *Clays and Clay Minerals*, **47**, 591–604.

Farmer, V.C. (1974) *The Infrared Spectra of Minerals*. Monograph **4**, Mineralogical Society, London, 539 pp.

Gaboriau, H. (1991) Interstratifiés smectite-kaolinite de l'Eure. Thesis, Université d'Orléans, 274 pp.

Gates, W.P., Slade, P.G., Manceau, A. and Lanson, B. (2002) Site occupancies by iron in nontronites. *Clays and Clay Minerals*, **50**, 223–239.

Glaeser, R. and Fripiat, J.J. (1976) Hydratation des smectites et démixtion des cations Li, Na en fonction de la localisation des substitutions isomorphiques. *Clay Minerals*, **11**, 93–99.

Goodman, B.A., Russell, J.D., Fraser, A.R. and Woodhams, F.W.D. (1976) A Mössbauer and IR spectroscopic study of the structure of nontronite. *Clays and Clay Minerals*, **24**, 53–59.

Greene-Kelly, L. (1955) Dehydration of montmorillonite minerals. *Mineralogical Magazine*, **30**, 604–615.

Guillaume, D., Neaman, A., Cathelineau, M., Mosser-Ruck, R., Peiffert, C., Abdelmoula, M., Dubessy, J., Villieras, F., Baronnet, A. and Michau, N. (2003) Experimental synthesis of chlorite from smectite at 300°C in the presence of

metallic Fe. *Clay Minerals*, **38**, 281–302.

Habert, B. (2000) Réactivité du fer dans les gels et les smectites. Thesis, Université Paris 6, Paris, 227 pp.

Hamilton, D.L. and Henderson, C.M.B. (1968) The preparation of silicate compositions by a gelling method. *Mineralogical Magazine*, **36**, 832–838.

Heller-Kallaï, L. (1975a) Interaction of montmorillonite with alkali halides. *Proceedings of the International Clay Conference*, Mexico, pp. 361–375.

Heller-Kallaï, L. (1975b) Montmorillonite-alkali halide interaction: a possible mechanism of illitization. *Clays and Clay Minerals*, **23**, 462–467.

Heller-Kallaï, L. (2001) Protonation-deprotonation of dioctahedral smectites. *Applied Clay Science*, **20**, 27–38.

Heller-Kallaï, L. and Mosser, C. (1995) Migration of Cu ions in Cu montmorillonite heated with and without alkali halides. *Clays and Clay Minerals*, **43**, 738–743.

Heller-Kallaï, L. and Rozenson, I. (1981) Nontronite after acid or alkali attack. *Chemical Geology*, **32**, 95–102.

Hillier, S. (2000) Accurate quantitative analysis of clay and other minerals in sandstones by XRD: comparison of a Rietveld and a reference intensity ratio (RIR) method and the importance of sample preparation. *Clay Minerals*, **35**, 291–302.

Hofmann, V. and Klemen, R. (1950) Verlust der Austauschfähigkeit von lithiumionen aus Bentonit durch Erhitzung. *Zeitschrift für Anorganische und Allgemeine Chemie*, **262**, 95–99.

Jaynes, W.F. and Bigham, J.M. (1987) Charge reduction, octahedral charge, and lithium retention in heated, Li-saturated smectites. *Clays and Clay Minerals*, **35**, 440–448.

Kamei, G., Oda, C., Mitsui, S., Shibata, M. and Shinozaki, T. (1999) Fe(II)-Na ion exchange at interlayers of smectite: adsorption-desorption experiments and a natural analogue. *Engineering Geology*, **54**, 15–20.

Kloprogge, J.T., Komarneni, S. and Amonette, J.E. (1999) Synthesis of smectite clay minerals: a critical review. *Clays and Clay Minerals*, **47**, 529–554.

Kohler, E. (2001) *Réactivité des mélanges synthétiques smectite/kaolinite et smectite/aluminium gel en présence d'un excès de fer métal*. DRT, Université d'Evry val d'Essonne, Evry, France, 101 pp.

Lantenois, S. (2003) Réactivité fer métal/smectites en milieu hydraté à 80°C. PhD thesis, Université d'Orléans, Orléans, France, 188 pp.

Madejová, J. and Komadel, P. (2001) Baseline studies of The Clay Minerals Society Source Clays: infrared methods. *Clays and Clay Minerals*, **49**, 410–432.

Madejová, J., Bujdak, J., Gates, W.P. and Komadel, P. (1996) Preparation and infrared spectroscopic characterization of reduced-charge montmorillonite with various Li contents. *Clay Minerals*, **31**, 233–241.

Madejová, J., Arvaiova, B. and Komadel, P. (1999) FTIR spectroscopic characterization of thermally treated Cu^{2+}, Cd^{2+} and Li$^+$ montmorillonites. *Spectrochimica Acta Part A*, **55**, 2467–2476.

Madejová, J., Bujdak, J., Petit, S. and Komadel, P. (2000a) Effects of chemical composition and temperature of heating on the infrared spectra of Li-saturated dioctahedral smectites. (I) Mid-infrared region. *Clay Minerals*, **35**, 739–751.

Madejová, J., Bujdak, J., Petit, S. and Komadel, P. (2000b) Effects of chemical composition and temperature of heating on the infrared spectra of Li-saturated dioctahedral smectites. (II) Near-infrared region. *Clay Minerals*, **35**, 753–761.

Mamy, J. (1968) Recherches sur l'hydratation de la montmorillonite: Propriétés diélectriques et structure du film d'eau. Thesis, Université de Paris 6, Paris, 142 pp.

McBride, M.B. and Mortland M.M. (1974) Copper (II) interactions with montmorillonite: Evidence from physical

methods. *Soil Science Society of America Proceedings*, **38**, 408−415.

Monier, G. and Robert, J.-L. (1986) Evolution of the miscibility gap between muscovite and biotite solid solutions with increasing lithium content: an experimental study in the system $K_2O-Li_2O-MgO-FeO-Al_2O_3-SiO-H_2O-HF$ at 600°C, 2 kbar p_{H_2O}: comparison with natural lithium micas. *Mineralogical Magazine*, **50**, 641−651.

Mosser, C., Michot, L.J., Villieras, F. and Romeo, M. (1997) Migration of cations in copper(II)-exchanged montmorillonite and Laponite upon heating. *Clays and Clay Minerals*, **45**, 789−802.

Norrish, K. (1954) The swelling of montmorillonite. *Discussions of the Faraday Society*, **18**, 120−134.

Palkova, H., Madejová, J. and Righi, D. (2003) Acid dissolution of reduced-charge Li- and Ni-montmorillonites. *Clays and Clay Minerals*, **51**, 133−142.

Pelletier, M., Michot, L.J., Humbert, B., Barres, O., D'espinose de la Callerie, J.B. and Robert, J.L. (2003) Influence of layer charge on the hydroxyl stretching of trioctahedral clay minerals: A vibrational study of synthetic Na- and K-saponites. *American Mineralogist*, **88**, 1801−1808.

Perronnet, M. (2001) Etude des interactions fer-argile en condition de stockage géologique profond des déchets nucléaires HAVL. DEA, ENS Géologie, Nancy, 33 pp.

Perronnet, M. (2004) *Etude des interactions fer-argile en condition de stockage géologique profond des déchets nucléaires HAVL*. PhD thesis, ENS Géologie, Nancy, France, 233 pp.

Pons, C.H., Rousseaux, F. and Tchoubar, D. (1981) Utilisation du rayonnement synchrotron en diffusion aux petits angles pour l'étude du gonflement des smectites: I. Etude du système eau-montmorillonite-Na en fonction de la température. *Clay Minerals*, **16**, 23−42.

Roux, J. and Volfinger, M. (1996) Mesures précises à l'aide d'un détecteur courbe. *Journal de Physique*, **IV**, 127−134.

Russell, J.D. (1979) An infrared spectroscopic study of the interaction of nontronite and ferruginous montmorillonites with alkali metal hydroxides. *Clay Minerals*, **14**, 127−137.

Russell, J.D. and Fraser, A.R. (1994) Infrared methods in clay mineralogy. Pp. 11−67 in *Spectroscopic and Chemical Determinative Methods* (M.J. Wilson, editor). Chapman & Hall, London.

Shannon, R.D. (1976) Revised effective ionic radii and systematic studies of interatomic distances in halides and chalcogenides. *Acta Crystallographica A*, **32**, 751−767.

Skipper, N.T., Chang, F.R.C. and Sposito, G. (1995) Monte Carlo simulation of interlayer molecular structure in swelling clay minerals. 1. Methodology. *Clays and Clay Minerals*, **43**, 285−293.

Suquet, H.B. (1978) Propriétés de gonflement et structure de la saponite. Comparaison avec la vermiculite. Thesis, Université Pierre et Marie Curie, Paris, 175 pp.

Suquet, H., IIyama, J.T., Kodama, H. and Pezerat, H. (1977) Synthesis and swelling properties of saponites with increasing layer charge. *Clays and Clay Minerals*, **25**, 231−242.

Suquet, H., Malard, C., Copin, E. and Pezerat, H. (1981) Variation du paramètre b et de la distance basale d_{001} dans une série de saponites à charge croissante: I Etats hydratés. *Clay Minerals*, **16**, 53−67.

Tomoe, Y., Shimizu, M. and Nagae, Y. (1999) Unusual corrosion of a drill pipe in newly developed drilling mud during deep drilling. *Corrosion*, **55**, 706−713.

Tournassat C., Charlet L. & Greneche J.-M. (2005) Interactions of Fe^{2+}, Zn^{2+}, and H_4SiO_4 at clay/water interfaces: Distinguishing sorption, coadsorption, and surface oxidation phenomena. *Geochimica et Cosmochimica Acta* (submitted).

Vantelon, D., Pelletier, M., Michot, L.J., Barres, O. and Thomas, F. (2001) Fe, Mg and Al distribution in the octahedral sheet of montmorillonites. An infrared study in the OH-bending region. *Clay Minerals*, **36**, 369−379.